Journal of Crystal Growth 354 (2012) 49–56

Contents lists available at SciVerse ScienceDirect

Journal of Crystal Growth

journal homepage: www.elsevier.com/locate/jcrysgro

A numerical model study of the effect of interface shape on particle pushing

Eliana M. Agaliotis, Carlos E. Schvezov, Mario R. Rosenberger *, Alicia E. Ares

CONICET-FCEQYN, UNAM, Azara 1552, (3300) Posadas—Misiones, Argentina

ARTICLE INFO

Article history:
Received 7 February 2012
Received in revised form
19 April 2012
Accepted 24 May 2012
Communicated by J. J. Derby
Available online 4 June 2012

Keywords:
A1. Computer simulation
A1. Interfaces
A1. Segregation
A1. Solidification

ABSTRACT

A numerical model using an axisymmetric approximation is developed to study particle pushing during solidification. The model is applied to determine the effect of different parameters on the predicted critical velocity for engulfment of the particle by the solidifying interface. The main parameters considered are particle radius, interface velocity and interface shape as obtained for different thermal conductivities between matrix and particle. The relative thermal conductivity is very important in the pushing/capture process in increasing or decreasing the critical velocity for pushing one order of magnitude, with respect to the critical velocity for a flat interface, depending on whether the interface is concave or convex. Moreover, the predicted critical velocities cover the span of measured values in agreement with the tendency given by the thermal conductivities and particle radius.

1. Introduction

The presence of particles in a material can enhance its properties as in the case of composites and alloy hardening with fine precipitates, or could be detrimental as in the case of large inclusions in steel and optic and electronic crystals. When the production process includes a solid–liquid interface as in the cases of precipitation from solution, electrolytic deposition and solidification, an interaction with the particles in the melt or solution may take place. During solidification the particles tend to segregate from the solid remaining in the last solidifying melt. This segregation is generally attributed to an interaction between the particles and the interface in which the interface pushes the particles. Nevertheless, the segregation could be the result of other processes such as fluid flow and particle flotation [1]. The conditions for pushing have been analyzed using basic thermodynamics considering the change in free energy [2–6]. However, a steady state of pushing is achieved after a transient where the interacting forces equilibrate. It is therefore important to know, describe and incorporate in the analysis the acting physical forces resulting from the interaction.

The pushing phenomenon has been investigated experimentally by using analytical and numerical modeling [1–45]. The physics of pushing has been extensively studied by Chernov and Temkin [12] and reviewed by Stefanescu [57]. The experiments made with transparent materials [1–7,11,40–45] such as water, naphthalene, salol and others containing different particle materials show that when the moving interface is able to push a particle, there is a critical velocity at which the particle can no longer be pushed and is trapped and engulfed by the interface. The critical velocity is inversely related to the particle size; the larger the particle the slower the critical velocity. Theories have been developed to relate the critical velocity with particle size, using different physical forces. The studies have shown that the pushing process is complex due to the variety of phenomena involved during pushing, its association to the fluid and thermal fields and the nature of the pushing force. In all cases, the physical problem depends on the properties, nature, and morphology of the interacting media, the particle, melt and solid, and external fields such as gravity, thermal and electromagnetic fields [14–28]. As a result, the scatter in the measurements as well as the amplitude of the range of velocities predicted from the models is large [32,37,39]. In view of this it becomes important to address the effect of each parameter independently in order to establish the importance in the phenomenon. One of the aspects which could be relevant is the effect of interface shape as determined by the difference in thermal conductivities among the particle, the melt and the solid. This effect has been considered qualitatively [10,46,47]; however the simple criteria of either relative thermal conductivities [46] or diffusivities [47] of particle and melt larger than one for trapping, failed when compared to experiments. More recent analytical and numerical modeling which include the effect of interface shape and thermal conductivity has been considered [21,25,29,30,47–52]. The numerical models were developed using a 2-D symmetry approximation. In the present report the results of a numerical model using axisymmetry is

* Corresponding author. Tel.: +54 376 4422186; fax: +54 376 4425414.
E-mail address: rrmario@fceqyn.unam.edu.ar (M.R. Rosenberger).

0022-0248/$ - see front matter © 2012 Elsevier B.V. All rights reserved.
http://dx.doi.org/10.1016/j.jcrysgro.2012.05.032

presented. With the model, the effect of different thermal conductivities between particle and matrix is considered which results in nonplanar interface shapes: convex and concave. The critical velocities for pushing as function of particle size is determined by employing the Lifshitz–van der Waals force as repulsive force, and the results are compared with the critical velocities for the case of a planar interface.

2. Model description

The particular physical situation which is analyzed basically consists of a spherical particle of radius R immersed in a melt and a solidifying interface moving towards the particle (Fig. 1). Also nonspherical particles are considered. The pushing and capture of a particle by a solid–liquid front are very complex and involve forces and conditions which strongly depend on the specific process as described in the literature [12]. In order to simplify the problem and focalize the effect of interface shape on capture, only two forces are considered, and these are the drag, which pushes the particle towards the interface, and the pushing force equilibrating the drag, which in the present case is the Lifshitz–Van der Waals force [1,8,9,12]. For the calculation of both forces, numerical methods based on the finite element method are developed assuming that the problem is axisymmetric.

The competition of the pushing or repulsion force (F_r) and drag force (F_d) determines whether a particle is pushed or captured. The equilibrium point occurs when both forces F_d and F_r are equal; the corresponding distance is the separation distance for steady state of pushing. The trapping condition applies when the separation distance between particle and interface reaches a minimum value of $h_{min}=1\times10^{-8}$ m, which is assumed to be the minimum thickness for a film to be considered as fluid [9,53,54]. This value was used in previous modeling [36] and is not considered as an adjusting parameter.

The equilibrium between drag and pushing forces is achieved at a specific separation distance; if this distance is larger than h_{min}, a steady state of pushing is possible, and if it is smaller than h_{min}, the particle is assumed to be trapped since the necessary flow for solidification is not possible.

To calculate the values of the drag and pushing forces it is necessary to know the interface shape as a function of the separation distance between particle and interface (h). Moreover, the pushing force is a function of h and R, and the drag force is a function of h, R and $v_{interface}$.

Since the interface shape below the particle is strongly and mainly dependent on the relative thermal conductivities of particle and matrix [10,46,47], the calculation of the temperature field is uncoupled in both the fluid flow field and pushing force calculations. First, the temperature field is calculated as a function of time and the interface shape is obtained for at least six different separation distances between particle and interface, and each shape is saved for later use. Second, the drag force onto the particle is calculated using the fluid flow field obtained with the model. Third, the repulsion force is calculated using the Casimir–Lifshitz–van der Waals model at each position.

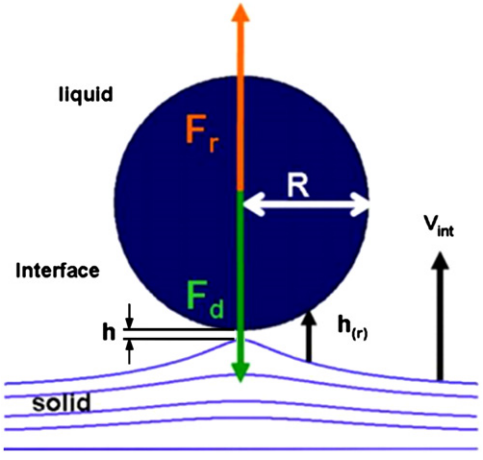

Fig. 1. Schematic description of particle pushing of a spherical particle.

Then the values of both forces $Fr(R,h)$ and $Fd(R,h,v_{interface})$ are compared using $v_{interface}$ as a parameter and the values of R and h are maintained constant, until both are equal. In such a case a set of R, h and $v_{interface}$ values for steady state of pushing is known. This method of calculation has been improved with respect to previous reports [31], adjusting both forces by logarithmic functions and finding $v_{interface}$ for steady state as the root of the resulting equation.

3. Results and discussion

The model was applied to conditions which produce planar, concave and convex interface shapes obtained by introducing in the model melt particles with three different relative conductivities kp/km of 1, 10 and 0.1. These relative values simulate the cases of k_{oxides}/k_{metals} with ratios ranging between 1.5 and 0.4 (e.g., $k_{Al_2O_3}/k_{Zn}=0.15$ and $k_{TiO_2}/k_{Al}=0.40$); $k_{ceramics}/k_{water}$ of around 10 (e.g., $k_{carbon\ fiber}/k_{water}=10.2$ or $k_{TiO_2}/k_{water}=12.3$); and around 1 for systems like mica/water, $k_{mica}/k_{water}=0.92$ and glass/water, $k_{glass}/k_{water}=1.25$ [55].The particle shapes considered were spherical and semi-spherical. In the first case the particle radii were 1, 10 and 50 μm, and in the second the radii were 10 and 50 μm. The growth velocities considered were in the range of 1×10^{-10}–1×10^{-4} m/s which covers the range of velocities normally present in many solidification processes where there may be a steady state of pushing.

3.1. Results of the temperature fields

The solidification domain including the particle is discretized assuming axisymmetric conditions around the particle axis which is parallel to the growth direction. A typical mesh consists of 50,000 quadrilateral elements with first order interpolation functions for the temperature field. To simulate the solidification process a constant heat flow is imposed in one side, equivalent to the heat flow generated by the solidification rate. The mesh is highly refined around the particle and particularly in the film between the particle and the boundary subjected to heat extraction. This procedure is applied in order to obtain a good resolution of the interface shape in the melt channel. The numerical solutions were obtained using a Newton–Raphson method with a tolerance of 0.01%. The dynamic time dependent part was solved by employing the Crank–Nicholson method with a variable time step adjusted by the Adams–Bashforth method [56]. The model is time dependent and permits to obtain the interface shape as it approaches the particle.

Comparing the results of the axisymmetric calculations with the results obtained with a 2D model where the particle is assumed to be an infinite cylinder, shown in Fig. 2, significant differences can be observed between the results of both approximations.

The figure shows the interface position at different times for the solidification of a melt in front of an infinite cylinder and a spherical particle in each case. The closest isotherms at a distance of 0.029 μm from the particle show the largest difference where it is observed that for the cylinder it is much closer to the surface

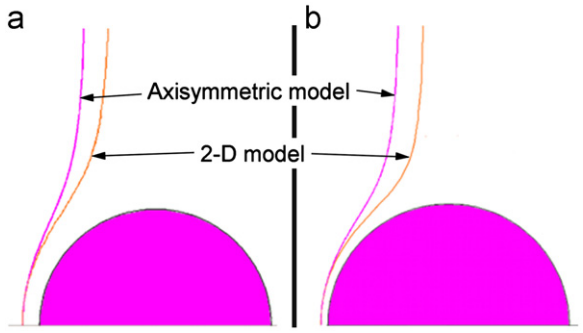

Fig. 2. Interface shapes obtained with the 2-D and the axisymmetric models at two particle–interface separation distances: (a) 7.3×10^{-6} m and (b) 2.9×0^{-6} m.

than the isotherm corresponding to the sphere for the same particle–interface separation. The separation h is measured at the closest approximation point between particle and interface which in the present case is in the symmetry plane or axis. The resulting drag force will be much larger for the cylindrical particle than for the spherical particle predicting the capture of the particle at much slower interface velocities for a given radius. Both the particle and cylinder radii are 50 μm, and the isotherms start to depart from each other at a distance of 222 μm or approximately 4 times the particle radius. On the other hand, the results also show that for distances between any particle and interface larger than $2R$ there is no effect of the particle on shape of the interface. In addition, the dimensional calculations show that the suitable non-dimensional or scaling parameter for the thermal field is $h/2R$ since the interfaces at equivalent positions given by the same value of $h/2R$ coincide exactly as expected.

The effect of the different thermal conductivities between particle and matrix in the interface shape is determined using three ratios of k_p/k_m of 10, 1 and 0.1. The resulting interface shapes are shown in Fig. 3a and b, noting that for the case of same conductivities the interface remains plane during the whole solidification process since the effect of fluid flow is not considered. In Fig. 3 it is observed that the shape is concave and convex for k_p/k_m of 10 and 0.1, respectively with a large curvature in both cases. In addition it is observed that the interface is not affected by the presence of the particle for distances larger than $2R$.

3.2. Results of the fluid flow fields

The fluid flow field is used to calculate the drag force onto the particle. The solidification process is simulated assuming there is a sink with the shape of the interface calculated with the temperature field model; the sink uniformly absorbs an amount of fluid equal to the amount of melt necessary to maintain a constant solidification velocity. Different meshes and approximations were previously employed to select the optimum between computing time and precision of the results. The domain was discretized using 30,000 and 50,000 quadrilateral elements, with second order interpolation functions for the velocity and first order for the pressure. The resulting system of equations was solved by employing the Picard method. The mesh in the fluid channel between particle and interface is highly refined as required. The viscosity of the melt was assumed to be constant and uniform with a value of 1.5×10^{-3} Pa s; the densities of the melt and particle were the same and equal to 2700 kg/m^3. The boundary condition on the particle surface was of no-slip and the range of interface velocity was from 1×10^{-10} m/s to 1×10^{-4} m/s; three particle radii, 50 μm, 10 μm and 1 μm; and six different values of h. The results show that the fluid flow is continuous around the particle with no separation lines, regular with a

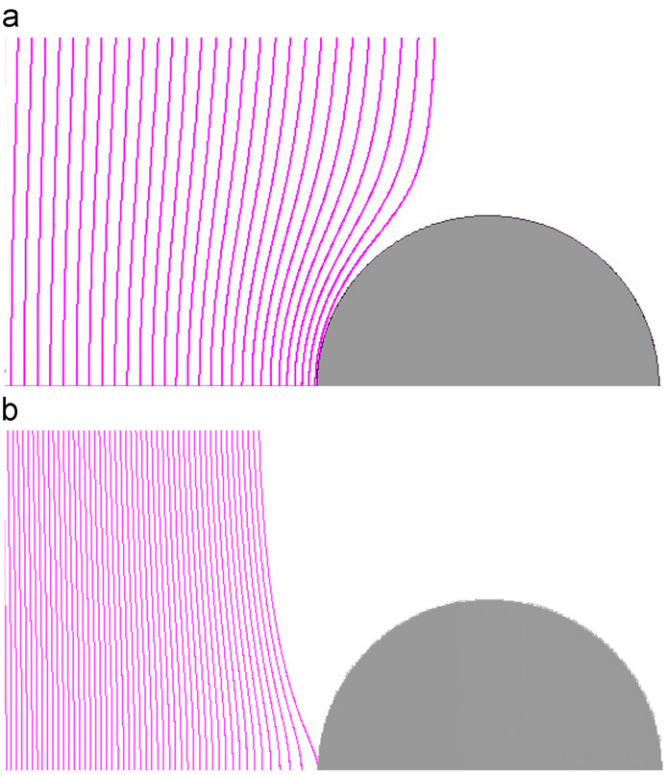

Fig. 3. Interface shapes at different separation distances from a spherical particle $R=50$ μm: (a) $k_P/k_L=10$, concave interface and (b) $k_P/k_L=0.1$, convex interface.

velocity that increases in the narrow gap between particle and interface.

It is noted that, for a given particle radius and interface velocity, fluid flow velocities are higher in the particle–interface channel for the case of the concave interface than for a flat interface, which in turn produce higher velocities than for the case of a convex interface. The higher velocities in the channel produce stronger drag forces as shown below.

3.3. Results of the drag force

The drag force on the particle due to fluid flow is calculated by integration of the following equation:

$$F_i=\int_S \varphi\vec{\sigma}\,dS=\int_S \varphi\sigma_{ij}n_j\,dS \tag{1}$$

where, F_i is the component of the force in the i-th direction, n_j is the versor in the j-th direction, σ_{ij} is the stress component, φ is the column vector of interpolation functions, dS is the differential surface; the integration is performed on the whole surface S of the particle.

The stress tensor σ is obtained from the velocity field using the following equation

$$t_i=\sigma_{ij}n_j,\sigma_{ij}=-p\delta_{ij}+\mu(u_{i,j}+u_{j,i}) \tag{2}$$

where p is the pressure term, μ is the viscosity and $u_{i,j}$ and $u_{j,i}$ are the velocity gradients of the i and j components in the j and i directions, respectively.

The drag forces as function of separation distance calculated for concave, flat and convex interfaces are shown in Fig. 4 for a particle 50 μm in radius, a solidification velocity of 3.3×10^{-8} m/s and thermal conductivities that produce concave, flat and convex interfaces. In the figure it is observed that the drag force in the

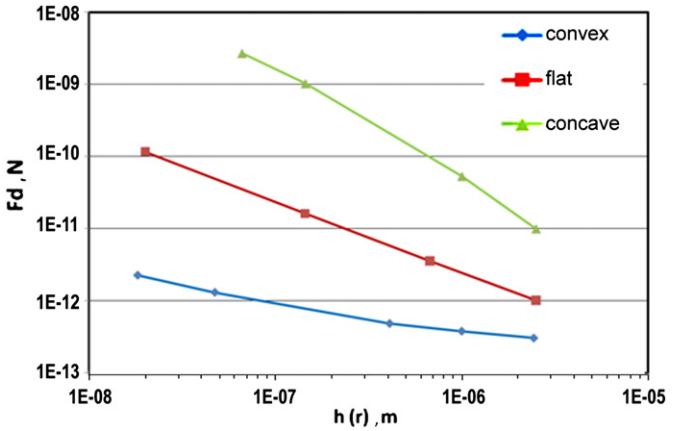

Fig. 4. Drag force as a function of separation distance for concave, flat and convex interface shapes onto a particle 50 μm in radius and a growth velocity of 3.3×10^{-8} m/s.

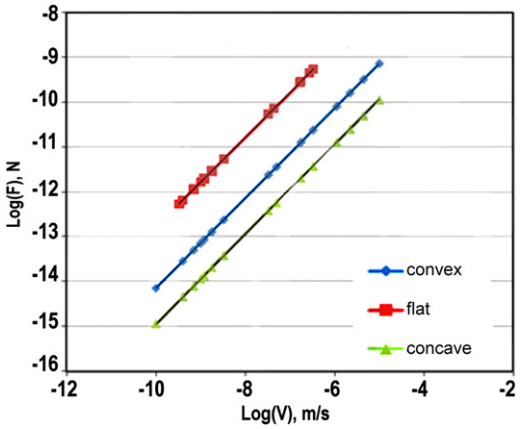

Fig. 5. Drag force versus solidification velocity for convex, flat and concave interface shapes, for a ratio $h/2R$ of 0.01.

case of a concave interface is two orders of magnitude larger than the corresponding force for the case of a flat interface at the same and small separation distance. In addition, as the separation distance increases, the force corresponding to the concave interface approaches the magnitude of the force corresponding to a flat interface; at a separation of two radii both forces are equal. On the other hand, in Fig. 4, the drag force for the case of a convex interface is two orders of magnitude smaller than the drag force for the case of a flat interface. As in the case of a concave interface the force is larger at small separation distances and the difference decreases and they become equal at a distance of two radii. In all cases, for a given solidification velocity and particle radius, the drag force for a concave interface is larger than the drag force for a flat interface and this, in turn, is larger than for a convex interface; in all cases the difference of drag force among the three decreases with increasing separation distance.

The effect of solidification velocity or fluid flow around the particle for the three cases, convex, flat and concave interface shapes produced by the different thermal conductivities between particle and matrix is shown in Fig. 5. It is observed that in the three cases or in other words, independent of the shape of the interface, the log (F_d) versus log (h) relation is linear and the lines are parallel to each other maintaining the relation of magnitude of the forces for the three interface shapes as described above. Moreover, the slopes of the linear functions are the same with a value of one, indicating in all the cases a linear relation in a logarithmic scale between drag force and fluid velocity. The log–log relations are of the type $\log(F_d)=\log(V)-b$; in such a case the direct relation between F_d and V is of the type $F_d=10^{-b}\times V=a\times V$. This relation holds for all the ranges of separation distances of interest for pushing and also for all particle radii considered in the present investigation. The value of a depends on separation distance, particle radius and particle–interface shape. The parameter a is the value of the drag force at a velocity of 1 m/s; see values in Table 1. It is noted that the drag force increases relatively more for the case of the concave interface than for the flat and the convex interfaces in that order, as the separation distance decreases.

In a previous report [31], the results of the calculated drag force for a planar interface were compared with the values given by two analytical equations which were the Stokes equation for a spherical particle and the modified Stokes equation, both shown in Eqs. 3 and 4. The results of the comparison showed that there is a large interval in which none of the approximations could be applied and that the transition point which separates the best fit of each analytical approximation is $h/R=1.0$. [31].

Table 1
Values of $\boldsymbol{a}$ in the fitting of $\boldsymbol{F=a.V}$ for three separation distances and different interface shapes.

Interface shape	$a\times10^5$ (kg/s)		
	$h\times10^6$ (m)		
	2.5	1	0.147
Concave	30.012	162.10	312.1
Flat	3.0633	7.2310	48.887
Convex	0.8972	1.1366	4.086

Table 2
Values of $f(R/h)$ as a function of R/h.

R/h	Concave	Flat	Convex
0	1	1	1
20	212.3	21.67	3.34
50	1146.6	51.15	8.04
340.13	2207.68	341.85	28.9

$$F_{dStokes}=6\pi\mu v_{\text{int}}R \tag{3}$$

$$F_{dS-M}=6\pi\mu v_{int}\frac{R^2}{h} \tag{4}$$

In view of this more general equations for the calculation of the drag force for the three cases are proposed as follows. In each case of combining and expanding the Stokes equation the following relation is proposed:

$$F_d=6\pi\mu vR\left[1+c_1\frac{R}{h}+c_2\left(\frac{R}{h}\right)^2\right]=6\pi\mu vRf\left(\frac{R}{h}\right) \tag{5}$$

where c_1 and c_2 are constants to be determined. From Fig. 5 it is possible to obtain the values shown in Table 2.

It is observed in Fig. 6a that for short distances compared to the particle radius the function f is linear with R/h and the transition starts for a value of 50, or $h=R/50$, which is a short distance between the particle and the concave interface. The two regimes can be fitted by a quadratic polynomial equation for long separation distances (Eq. (6a)), and a linear equation for the short

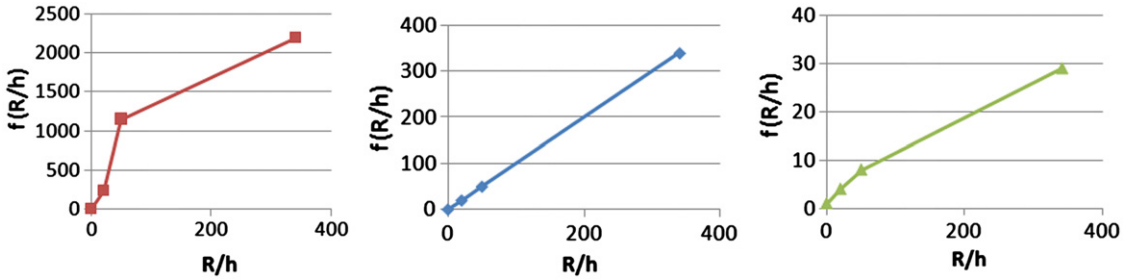

Fig. 6. $f(R/h)$ as a function of R/h showing the transition from large to small values of h (a) for a concave interface, (b) for a flat interface and (c) for a convex interface.

distances (Eq. (6b))

$$F_d = 6\pi\mu v R\left[1+2.3337\frac{R}{h}+0.4116\left(\frac{R}{h}\right)^2\right] \text{for}\left(\frac{R}{h}\right)<50 \quad (6a)$$

$$F_d = 6\pi\mu v R\left[254.98+1.703\frac{R}{h}\right] for\left(\frac{R}{h}\right)>50 \quad (6b)$$

For the case of a flat interface the relation of f with R/h is perfectly linear as observed in Fig. 6b; the fitting relation is

$$f\left(\frac{R}{h}\right)=1.0022\left(\frac{R}{h}\right)+1 \quad (6c)$$

which shows that the equation

$$F_d = 6\pi\mu v R\left[1+\frac{R}{h}\right] \text{forall}\left(\frac{R}{h}\right) \quad (6d)$$

is a general equation for the pushing force for a flat interface covering the whole range of values of R and h and includes the transition from short to long separation distances.

In the case of a convex interface the relation of f versus R/h is shown in Fig. 6c where it is possible to distinguish the two regions for long and short distances. The equations for each region are shown in Eqs. (6d and 6e).

$$F_d = 6\pi\mu v R\left[1+0.1011\frac{R}{h}+0.0008\left(\frac{R}{h}\right)^2\right] for\left(\frac{R}{h}\right)<50 \quad (6e)$$

$$F_d = 6\pi\mu v R\left[4.4451+0.0719\frac{R}{h}\right] for\left(\frac{R}{h}\right)>50 \quad (6f)$$

Analyzing the five above equations it is observed that for the three cases at a short distance there is a linear relation with R/h; however the slope or multiplying constant changes from one case to the other. In first place the coefficient is one for a flat interface, larger than one for a concave interface of 1.703, and much smaller for a convex interface of 0.0719.

3.4. Results of the pushing force

The pushing force is calculated using an equation which corresponds to the Lifshitz–van der Waals equation for short distances, where B_3 is the Lifshitz–van der Waals constant and $h(r)$ is the separation distance between the particle and interface as indicated in Fig. 1.

$$F_r = 2\pi B_3\int_0^R \frac{r}{h^3(r)}\,dr \quad (7)$$

The values of pushing or repulsive force calculated using the above equation are shown in Fig. 7 for a particle 50 μm in radius and for the three shapes of interface considered: concave, flat and convex. It is observed that in a logarithmic scale the force, for the three interface shapes, depends linearly onseparation distance in an inverse way. Similar results are obtained for smaller particle radius. Potential regression fitting performed for the cases

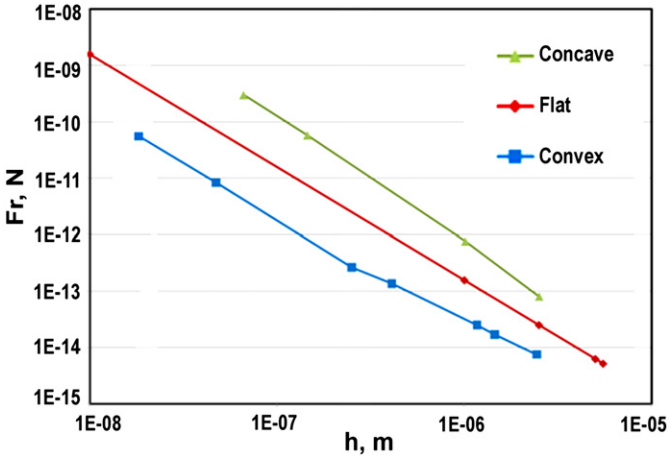

Fig. 7. Pushing or repulsive force calculated numerically for a particle 50 μm in radius and for the three shapes of interface considered: concave, flat and convex.

Table 3
Values of the parameters ***B*** and ***n*** for three interface shapes and different particle radii.

Interface	R (μm)	B (N μm^n)	n
Concave	50	8.58×10^{-28}	2.477
	1	2.70×10^{-30}	2.482
Flat	50	3.14×10^{-27}	2.0
	1		
Convex	50	9.44×10^{-25}	1.761
	1	6.78×10^{-25}	1.606

considered reproduced the analytical expresion obtained for a planar interface and a spherical particle as

$$F_r = \pi B_3\frac{R}{h^2} \quad (8)$$

The above equation could be genealized for the case of concave and convex interfaces proposing potential functions of the type

$$F_r = \frac{B}{h^n} \quad (9)$$

The values of the parameters B and n which fit the numerical calculations in such a case are shown in Table 3 for particle sizes of 50 and 1 μm. In all cases the fitting is very good with a Pearsons Coefficient (R^2) greater than 0.99. In the case of a planar interface the value of 2 is perfectly reconstructed showing a good numerical integration procedure.

In the table it can also be seen that in the case of a convave interface the n exponent has the largest value, and also the value of B which is related to the particle radius; however it is not

possible to determine the analytical relation due to the small number of particle radii considered.

3.5. Equilibrium conditions and critical velocities

The equilibrium conditions for pushing are obtained equilibrating the two opposite forces: the drag and the repulsive forces. This can be done by equating the equations for drag and repulsive forces which were fitted with potential functions. Alternatively, the equilibrium position can be obtained numerically for each particle radius and each separation distance between particle and interface and searching numerically the fluid or solidification velocity which produces a drag force which equilibrate the repulsive force. The convenience of this procedure is that the pushing force is independent of solidification velocity and remains constant during the search of the equilibrium conditions.

The procedure is repeated for different separation distances, particle radii and interface geometries. For a flat interface and several particle radii the equilibrium separation distances versus velocity are shown in Fig. 8 for particle radii ranging from 1 to 50 μm. It is noted that at small equilibrium distances all the lines are parallel and linear and as the solidification velocity decreases the lines start to curve towards the abscissa, in particular for the case of the particle with the smallest radius of 1 μm. This larger separation is due to the larger separation between particle and interface for which case the drag force calculated numerically deviates from the approximation given by the modified Stokes equation which predicts smaller drag forces than those calculated numerically. Using the approximation of the modified Stokes equation will result in linear relations in a logarithmic scale representation of *heq* versus *Veq* [34,36,38].

The critical velocity for pushing is obtained as the point at which each line intercepts the abcisa which corresponds to a value of separation distance equal to the minimum of 10^{-8} m as previously described. The critical velocity is observable or experimentally measured and may be compared with those predicted by the model; this is done below.

In the case of a concave interface the equilibrium distance versus solidification velocity for three particle radii are shown in Fig. 9.

For comparison purposes the corresponding equilibrium distances for a flat interface are also shown. First, it is observed that at small velocities the corresponding larger equilibrium distances converges to those of a flat interface for all particle radii. This is the result of the larger curvature for longer separation distances where the drag and repulsive forces converge to those corresponding to a flat interface. For all particle radii at larger velocities the equilibrium distances are smaller which results in a critical velocity slower than for the case of a flat interface.

On the contrary, for the case of a convex solidification interface the equilibrium separation distance for pushing for a given velocity is larger than for either a flat or concave interface, as observed in Fig. 10.

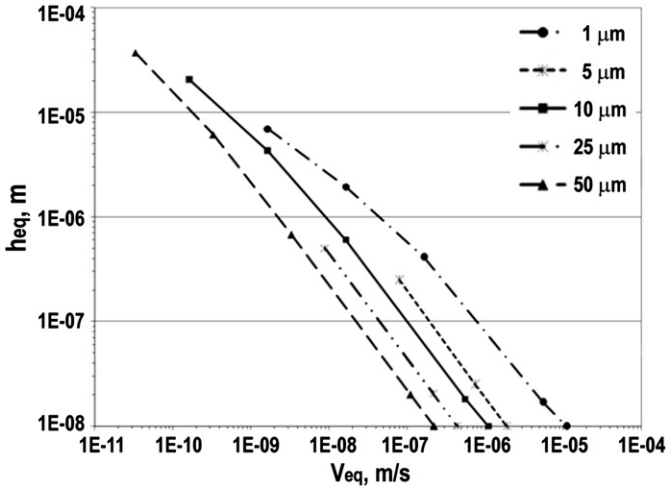

Fig. 8. Equilibrium separation distance for steady pushing as function of solidification velocity for a flat interface.

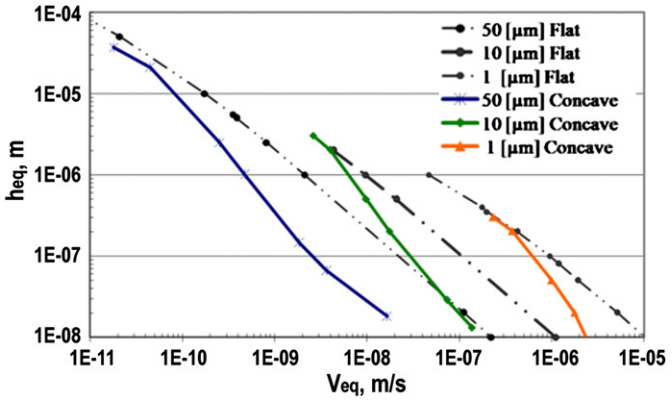

Fig. 9. Equilibrium separation distance for steady pushing as function of solidification velocity for concave interface shapes.

3.6. Critical velocities por pushing

The critical velocities for pushing are obtained from Figs. 8–10 and correspond to the velocity at which the line intercepts the abscise for an equilibrium distance $h_{\min}=10^{-8}$ m. The results for a water matrix and a flat interface are shown in Fig. 11; in the same figure the critical velocities obtained using the analytical equation (Eq. 10) are represented as a dashed line.

$$v_c = \frac{B_3}{6\pi h_{\min} R} \tag{10}$$

The conversion of critical velocities from one melt to another is straightforward and can be done using the simple following conversion equation

$$v_{c(\text{water})} = v_{c(\text{sim})} \left(\frac{\mu_{(\text{sim})}}{\mu_{(\text{water})}} \right) \tag{11}$$

Where μ_{sim} is the viscosity used in the model and $v_{c(\text{sim})}$ is the critical velocity obtained with the model for that viscosity.

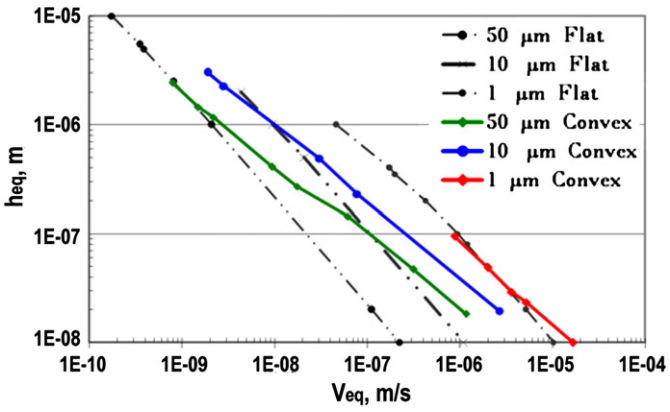

Fig. 10. Equilibrium separation distance for steady pushing as function of solidification velocity for convex interface shapes.

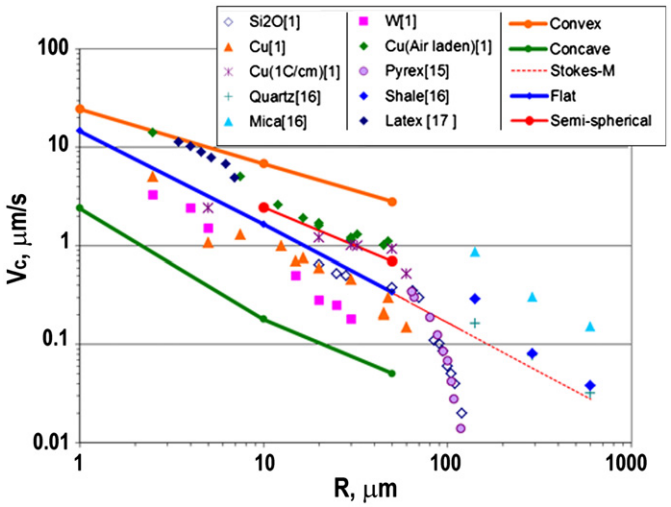

Fig. 11. Comparison between measured critical velocities and model predictions for flat, concave and convex interface shapes as function of particle radius.

In Fig. 11 the analytical and numerical results for a flat interface are practically coincident. In addition, the large scatter of experimental values is observed. When the effect of a curved interface is considered, the model results show the upper and lower limits enveloping the experimental values indicating that the experimental scatter can be partially explained by this fact. Another variable which can affect the critical velocity is the shape of the particle. To estimate the degree of importance of a non-spherical particle, the model was applied to a semi-spherical particle with the flat face parallel to the interface and in the upper part, that is, the spherical part facing the interface. The particle is insulating with respect to the matrix with a thermal conductivity a tenth of that of the matrix. In such a case the shape of the interface is convex. The results for two radii of 10 and 50 μm are included in Fig. 11, and show that the critical velocities for these cases are larger than the critical velocities for a flat interface and approximately 5 times smaller than the corresponding critical velocity for a spherical particle with the same radius and relation between thermal conductivities. In such a case it may be concluded that the upper and lower lines represent the limiting bounds for the critical velocities for pushing. If the model results are compared with some of the specific experimental cases, it may be noted that the metallic particles like tungsten and copper, with large thermal conductivities than water, have critical velocities smaller than those corresponding to a flat interface following the tendency of the model predictions. Moreover, in the case of copper particles in water solidified with a very low gradient where the effect of different thermal conductivities is smaller, the critical velocities are in some cases larger and in other cases smaller than the corresponding critical velocity for a flat interface. One significant observation is with respect to the case of air laden copper particles which show critical velocities corresponding to particles with smaller thermal conductivity than the matrix. An air laden particle will result in a mean thermal conductivity that could be smaller than those of copper and water.

4. Summary and conclusions

In the present report a simple model for pushing is presented in which two acting forces are considered: the drag force and the pushing force. The parameters and physical conditions analyzed are particle radius, growth velocity and different thermal conductivities of particle and matrix. Both forces are calculated using numerical methods and the results are analyzed for each physical condition producing flat, concave and convex interfaces. In addition the drag force is compared with analytical approximations and a more general equation is obtained which is valid for all cases of spherical particles and a flat interface. Also for all the cases, the drag and pushing forces are fitted to potential functions which permit to obtain the equilibrium position of a particle moving ahead of a solidifying interface. The trapping condition applied is that when the separation distance between particle and interface reaches a minimum value of 10^{-8} m. The results obtained with the model are compared to published experimental critical velocities measured for water and a considerable number of particle sizes and nature with smaller and larger thermal conductivities than the matrix. The analysis and discussion of the results permit to obtain the following conclusions.

(1) The axisymmetric approximation results are much more adequate than the 2-D approximation for the prediction of the interface shape for studying pushing, when the thermal conductivities between the foreign particle and the solidifying matrix are different.
(2) For foreign particles with larger or smaller thermal conductivities than that of the matrix, concave or convex interface shapes are obtained, respectively, as a function of distance between particle and interface. For separations larger than a particle diameter there is no effect on interface shape, remaining essentially planar.
(3) An analytical equation for the drag force is reconstructed from the numerical values of drag force valid for the whole range of separation distances between a spherical particle and a flat interface or sink, replacing in a continuous way both, the Stokes and the modified Stokes equations.
(4) The Lifshitz–van der Waals pushing force is integrated numerically for each interface particle separation and the analytical equation for a flat interface is perfectly reconstructed.
(5) The drag and the pushing forces are strongly dependent on interface shape and their magnitude could be as high as one order of magnitude larger following the inverse relation between thermal conductivities of particle and matrix.
(6) The drag and the pushing forces calculated numerically as function of particle radius, solidification velocity and thermal conductivities are fitted to polynomial functions permitting an easy calculation of the equilibrium distance between particle and interface for steady pushing.
(7) The equilibrium distance predicted numerically as function of particle radius and a flat interface fitted a linear inverse relation to the radius and velocity coinciding with published analytical relations.
(8) From the equilibrium position obtained as function of particle radius, solidifcation velocity and thermal conductivities, the critical velocity for pushing predicted with the model shows a range of up to one order of magnitude higher and lower than the corresponding critical velocity for a flat interface, depending on whether the thermal conductivity of the particle is lower or higher than that of the matrix, respectively.
(9) The critical velocities predicted with the model when compared with critical velocities measured experimentally in a wide range of conditions show that the predicitons cover almost all the measured values and are in agreement with the tendency given by the thermal conductivities and the particle radius.

References

[1] C.E. Schvezov, F. Weinberg, Interaction of iron particles with a solid-liquid interface in lead and lead-alloys, Metallurgical Transactions B 16 (1985) 367–375.

[2] C.E. Schvezov, Interaction of Iron Particles with a Solid-Liquid Interfase in Lead and Lead-Alloys, M.A.Sc. Thesis, Departent of Metals and Materials Engineering, UBC, Canada, 1983.
[3] D.R. Uhlmann, B. Chalmers, K.A. Jackson, Interaction between particles and a solid-interface, Journal of Applied Physics 35 (1964) 2986–2993.
[4] A.W. Neumann, J. Szekely, E.J. Rabenda (Jr), Thermodynamics of particle engulfment by solidifying melts, Journal of Colloid and Interface Science 43 (1973) 727–732.
[5] A.W. Neumann, D.J. van Oss1, J. Szekely, Thermodynamics of particle engulfment, Kolloid ZUZ Polymere 251 (1973) 415–423.
[6] S.N. Omenyi, A.W. Neumann, Thermodynamic aspects of particle engulfment by solidifying melts, Journal of Applied Physics 47 (1976) 3956–3962.
[7] M.V. Pikunov, The behavior of suspended impurities during crystallization. Non-ferrous metals, their treatment and working, Metallurgizdat, Moscow, 1957, pp. 56–67.
[8] E. Dzyaloshinskii, E.M. Lifshitz, L.P. Pitaevskii, General theory of van der Waals forces, Soviet Physics USPEKHI 72 (1961) 153–176.
[9] A.A. Chernov, D.E. Temkin, S.M. Mel'nikova, Theory of the capture of solid inclusions during the growth of crystals from the melt, Soviet Physics Crystallography 21 (4) (1976) 369–379.
[10] G.F. Bolling, J. Cisse, A theory for the interaction of particles with a solidifying front, Journal of Crystal Growth 10 (1971) 56–66.
[11] J. Cisse, G.F. Bolling, A study of the trapping and rejection of insoluble particles during the freezing of water, Journal of Crystal Growth 10 (1971) 67–76.
[12] A.A. Chernov, D.E. Temkin, Crystal Growth and Materials, in: E. Kaldis, H.J. Sheel (Eds.), North Holland, Amsterdan, 1976, p. 1977.
[13] D. Shangguan, S. Ahuja, D.M. Stefanescu, An analytical model for the interaction between an insoluble particle and an advancing solid/liquid interface, Metallurgical Transactions A. 23 (1992) 669–680.
[14] Y. Fasoyinu, C.E. Schvezov, Interaction of ceramic particles with an advancing solid–liquid interface in aluminum-based composites, in: Proceedings of the F. Weinberg International Symposium on Solidification Processing, Pergamon, 1990, p. 243.
[15] H. Shibata, H. Yin, S. Yoshinaga, T. Emi, M. Sizuki, In-situ observation of engulfment and pushing of nonmetallic inclusions in steel melt by advancing melt/solid interface, ISIJ International 38 (1998) 149–156.
[16] Q. Han, J.D. Hunt, Particle pushing: critical flow rate required to put particles into motion, Journal of Crystal Growth 152 (1995) 221–227.
[17] S. Chang, D.M. Stefanescu, A model for inverse segregation: the case of directionally solidified Al–Cu alloys, Acta Materialia 44 (1996) 2227–2235.
[18] S. Sen, B.K. Dhindaw, D.M. Stefanescu, A. Catalina, P.A. Curreri, Melt convection effects on the critical velocity of particle engulfment, Journal of Crystal Growth 173 (1997) 574–584.
[19] J.K. Kim, P.K. Rohatgi, The effect of the diffusion of solute between the particle and the interfase on the particle pushing phenomena, Acta Materialia 46 (1998) 1115–1123.
[20] S. Sen, F. Juretzko, D.M. Stefanescu, B.K. Dhindaw, P. Curreri, In situ observations of interaction between particulate agglomerates and an advancing planar solid/liquid interface microgravity experiments, Journal of Crystal Growth 204 (1999) 238–242.
[21] A.V. Catalina, S. Mukherjee, D.M. Stefanescu, A dynamic model for the interaction between a solid particle and an advancing solid/liquid interface, Metallurgical and Materials Transactions A: Physical Metallurgy and Materials Science 31 (2000) 2559–2568.
[22] V. Andris, V. Bune, S. Sen, S. Mukherjee, A. Catalina, D.M. Stefanescu, Effect of melt convection at various gravity levels and orientations on the forces acting on a large spherical particle in the vicinity of a solidification interface, Journal of Crystal Growth 211 (2000) 446–451.
[23] A.W. Rempel, M.G. Worster, Particle trapping at an advancing solidification front with interfacial-curvature effects, Journal of Crystal Growth 223 (2001) 420–432.
[24] H.S. Udaykumar, L. Mao, Interface simulations of dendritic solidification of solution, International Journal of Heat and Mass Transfer 45 (2002) 4793–4808.
[25] L. Hadji, Modelling and asymptotic analysis of particle-interface interaction, Mathematical and Computer Modelling 36 (2002) 147–156.
[26] J.W. Garvin, H.S. Udaykumar, Particle–solidification front dynamics using a fully coupled approach, part I: methodology, Journal of Crystal Growth 252 (2003) 451–466.
[27] J.W. Garvin, H.S. Udaykumar, Particle-solidification front dynamics using a fully coupled approach, part II: comparison of drag expressions, Journal of Crystal Growth 252 (2003) 467–479.
[28] M. Kolbe, X.R. Liu, T. Volkmann, R. Röstel, P.K. Galenko, G. Eggeler, B. Wei, D.M. Herlach, Interaction of solid ceramic particles with a dendritic solidification front, Materials Science and Engineering 375 (2004) 524–527.
[29] J.W. Garvin, H.S. Udaykumar, Drag on a particle being pushed by a solidification front and its dependence on thermal conductivities, Journal of Crystal Growth 267 (2004) 724–737.
[30] J.W. Garvin, Y. Yang, H.S. Udaykumar, Multiscale modeling of particle-solidification front dynamics. part II: pushing-engulfment transition, International Journal of Heat and Mass Transfer 50 (2007) 2969–2980.
[31] E.M. Agaliotis, M.R. Rosenberger, A.E. Ares, C.E. Schvezov, Numerical calculation of the drag force applied to particle pushing, Journal of Crystal Growth 310 (2008) 1366–1370.
[32] M.R. Rosenberger, E.M. Agaliotis, C.E. Schvezov, Modelización numérica de la interacción de partículas con una interfase de solidificación, Mecánica Computacional 24 (2005) 137–150.
[33] M.R. Rosenberger, E.M. Agaliotis, C.E. Schvezov, Modelización de la interacción de partículas con interfases de solidificación, Anales AFA 17 (2005) 228–233.
[34] M.R. Rosenberger, E.M. Agaliotis, C.E. Schvezov, Numerical modeling of interaction of particles with solidifying interfaces, in: N Gupta, W Hunt (Eds.), The Rohatgi Honorary Symposium on Solidification Processing of Metal Matrix Composites, Eds.,TMS, Texas, 2006.
[35] E.M. Agaliotis, M.R. Rosenberger, C.E. Schvezov, A.E. Ares, Analysis of the interaction of particles with non-planar solidifying interface, in light metals, in: Ed.,in: DD Young (Ed.), Cast Shop Technology, 3, TMS, 2008, p. 823.
[36] C.E. Schvezov, Dynamic Calculations for Particle Pushing, in Solidification, in: WH Hofmeister, et al., (Eds.), Eds.,TMS, USA, 1999, pp. 251–261.
[37] E.M. Agaliotis, M.R. Rosenberger, A.E. Ares, C.E. Schvezov, Modeling the interaction of particles with a concave solidifying interface, in: Proceedings of the XII Modeling of Casting, Welding and Advanced Solidification Process, 2009, pp. 209–217.
[38] C.E. Schvezov, Comparison between theory and experiments on particle pushing, Anales de Química Argentina 84 (5) (1996) 527–530.
[39] P. Hoekstra, D.R. Miller, The mobility of water molecules in the transition layer between ice and a solid interface, Journal of Colloid and Interface Science 25 (1967) 166–173.
[40] J. Cisse, G.F. Bolling, The steady-state rejection of insoluble particles by salol grown from the melt, Journal of Crystal Growth 11 (1971) 25–28.
[41] K.H. Chen, W.R. Wilcox, Anomalous influence of body force on trapping of foreign particles during solidification, Journal of Crystal Growth 40 (1977) 214–220.
[42] V.H.S. Kuo, W.R. Wilcox, Particle Chromatography, Separation Science 8 (1973) 375–377.
[43] R.H. Ewing, The free energy of the crystal-melt interface from the radial distribution function-further calculations, Philosophical Magazine 25 (1972) 779–784.
[44] A.E. Corte, Vertical migration of particles in front of a moving freezing plane, Journal of Geophysical Research 67 (3) (1962) 1085–1090.
[45] A.M. Zubko, V.G. Lobanov, V.V. Nikonova, Reaction of foreign particles with a crystallization front, Soviet Physics-Crystallography 18 (2) (1973) 239–241.
[46] M.K. Surappa, P.K. Rohatgi, Heat diffusivity criterion for the entrapment of particles by a moving solid–liquid interface, Journal of Materials Science 16 (2) (1981) 562–564.
[47] R. Sasikumar, T.R. Ramamohan, B.C. Pai, Critical velocities for particle pushing by moving solidification fronts, Acta Metallurgica 37 (7) (1989) 2085–2091.
[48] A.W. Rempel, M.G. Worster, The interaction between a particle and an advancing solidification front, Journal of Crystal Growth 205 (3) (1999) 427–440.
[49] J.W. Garvin, H.S. Udaykumar, Drag on a ceramic particle being pushed by a metallic solidification front, Journal of Crystal Growth 276 (2005) 275–280.
[50] J.W. Garvin, Y. Yang, H.S. Udaykumar, Multiscale modeling of particle–solidification front dynamics, part I: methodology, International Journal of Heat and Mass Transfer 50 (2007) 2952–2968.
[51] J.C.T. Kao, A.A. Golovin, S.H. Davis, Particle capture in binary solidification, Journal of Fluid Mechanics 625 (2009) 299–320.
[52] L. Hadji, A.M.J. Davis, The influence of insoluble spherical particles on the stability of a planar solidifying interface, Journal of Crystal Growth 191 (1998) 889–896.
[53] K.V. Sharp, R.J. Adrian, Transition from laminar to turbulent flow in liquid filled microtubes, Experiments in Fluids 36 (2004) 741–747;
K.V. Sharp, R.J. Adrian, Transition from laminar to turbulent flow in liquid filled microtubes, Experiments in Fluids 38 (1) (2005) 132.
[54] K. Travis, B. Todd, D. Evans, Departure from Navier–Stokes hydrodynamics in confined liquids, Physical Review E 55 (1997) 4288–4295.
[55] Y. Cengel, Heat and Mass Transfer: A Practical Approach, 3rd ed., Mc Graw-Hill, 2006.
[56] S.C. Chapra, R.P. Canale, Numerical Methods for Engineers, McGraw-Hill, 2005.
[57] D.M. Stefanescu, Behavior of Insoluble Particles at the Solid/Liquid Interface, 9th ed.,Metals Handbook, 15, ASM Handbook, 1988, pp. 315–326.